

The properties of the Galactic Hard X-Ray and soft γ -ray Background based on 20 years of INTEGRAL/IBIS observations

Roman Krivonos^a, Ekaterina Shtykovskaya^a, Sergey Sazonov^a

^aSpace Research Institute of the Russian Academy of Sciences, Profsoyuznaya 84/32, Moscow, 117997, , Russia

Abstract

In this work we present results of a study of the Galactic hard X-ray and soft γ -ray background emission performed with the *IBIS* telescope aboard *INTEGRAL* observatory using data obtained over more than 20 years of operations. The study of Galactic background at energies between 10 keV and a few MeV is problematic due to the contribution of point sources, high instrumental background and large-scale extent of the emission, which leads to the need of utilizing complex model-dependent methods. Using the unique properties of the *IBIS* coded-mask telescope, we developed model-independent approach to study diffuse continuum emission within the Galactic plane in 25–60, 60–80, and 80–200 keV bands. The comparison of 25–60 keV longitude profile with near infrared intensity shows excellent agreement, confirming stellar origin of Galactic Ridge X-ray Emission (GRXE). The Galactic X-ray background is significantly detected in the Galactic bulge region up to 200 keV. We build broad-band spectra of the Galactic background in three broad regions, the Galactic bulge and two spiral arms at $l \approx \pm 20^\circ$. The spectral analysis reveals two distinct components with a minimum at about 80 keV. The low-energy component $E \lesssim 60$ keV, coming from GRXE, is consistent with a one-dimensional accretion flow model of intermediate polars with an average white dwarf mass of about $0.7 M_\odot$. The high-energy part of the spectrum, attributed to γ -ray background at $E \gtrsim 80$ keV is consistent with a power-law model with photon index $\Gamma = 1.55$. The total 30–80 keV flux budget of $1.5 \times 10^{-9} \text{ erg s}^{-1} \text{ cm}^{-2}$ observed within effective *IBIS* FOV ($\approx 286 \text{ deg}^2$) in the region of Galactic bulge, consists of 2/3 of GRXE and 1/3 of γ -ray background. Finally, we provide the Python code of the *IBIS/ISGRI* background model, which can be used to measure the X-ray intensity of the Galactic background in different parts of the Milky Way.

Keywords: X-rays: general, Galaxy: bulge, Galaxy: general, gamma rays: diffuse background, X-rays: diffuse background

1. Introduction

The stellar origin of the Galactic ridge X-ray emission (GRXE), has been strongly supported by morphological study with RXTE observatory in a pioneering work by Revnivtsev et al. (2006), who have shown that the 3–20 keV map of the GRXE closely follows the near-infrared brightness distribution of the Galaxy and thus traces the Galactic stellar mass distribution. Revnivtsev et al. (2006) also predicted high-energy cut-off in the spectrum of GRXE above 20 keV, later observed with *INTEGRAL* (Krivonos et al., 2007; Türler et al., 2010; Bouchet et al., 2008, 2011; Siegert et al., 2022), *Suzaku* (Yuasa et al., 2012) and *NuSTAR* (Perez et al., 2019). GRXE is associated with old stellar population of the Galaxy, namely with hard X-ray emission from accreting white dwarfs – polars and intermediate polars, the main population contributing to it. The accretion column onto the magnetic poles of such types of accreting white dwarfs is emitting optically thin thermal emission. The integrated emission of a large number of such faint Galactic X-ray sources constitute the observed GRXE (see e.g., Revnivtsev et al., 2008; Revnivtsev et al., 2009; Revnivtsev et al., 2011; Lutovinov et al., 2020).

In contrast to GRXE, the Galactic Diffuse Continuum Emission (GCDE) at energies above 100 keV is considered as truly diffuse in origin. GCDE at energies below ≈ 70 MeV is mainly

due to the interactions of cosmic-rays (CR) with the interstellar material and radiation fields (Kraushaar et al., 1972; Kniffen et al., 1978; Hunter et al., 1997). The Compton scattering of the CR leptons with the interstellar radiation field and the cosmic microwave background is the major contribution to GCDE (Porter and Strong, 2005; Porter et al., 2008). Observations of Galactic γ -ray diffuse emission thus provide a unique opportunity to study the properties of Galactic CR particles (Bouchet et al., 2011; Siegert et al., 2022; Karwin et al., 2023).

However, the detection of high-energy Galactic emission has always been a very difficult problem. The signal is very weak and thus strongly depends on the accuracy of the instrumental background subtraction. A number of detections and non-detections of high-energy Galactic emission have been claimed (e.g. Riegler et al., 1985; Kinzer et al., 2001; Strong et al., 2005; Bouchet et al., 2008). Another difficulty is unknown spatial distribution of cosmic-ray induced background, which leads to the need of using complex model-dependent methods (e.g., Bouchet et al., 2011; Siegert et al., 2022). Therefore, any independent study of the Galactic background in hard X-ray and soft γ -ray band is important to improve our understanding of energetic content of the Milky Way.

Thanks to the unique combination of properties of *INTEGRAL* *IBIS* and *SPI* telescopes – broad band coverage, large

fields of view and possibilities to eliminate the contribution of discrete sources from the total measured photon flux, the study of the Galactic hard X-ray and soft γ -ray Background is possible. The aim of this work is to provide model-independent measurements of the wide-angle morphology and broad band spectrum of the Galactic background emission above 25 keV up to 200 keV with *IBIS* telescope.

The paper is organized as follows. Section 2 describes multi-year *INTEGRAL* all-sky observations and initial data reduction. Section 3 presents the concept of using *IBIS* telescope as a collimated instrument for studying Galactic large-scale X-ray emission. The details of the method, namely the description of the *IBIS* detector background model and flux calibration with Crab Nebula, respectively, can be found in Appendix A and Appendix B. The results are present in Section 4, where flux measurement in different Galactic regions (Section 4.1); longitude morphology in different energy bands up to 200 keV (Section 4.2); and spectral analysis (Section 4.3) of Galactic emission can be found.

2. Observations and data reduction

For this work we use all publicly available *INTEGRAL* (Winkler et al., 2003) data acquired with the *IBIS* coded-aperture telescope (Ubertini et al., 2003) from May 2003 to February 2024 (orbits 70–2740). We considered only the data of the *ISGRI* detector (Lebrun et al., 2003), which provides data in the energy band 17–1000 keV with high sensitivity in the transition interval from hard X-rays to soft γ -rays (17–200 keV).

We reduced *IBIS/ISGRI* data with a proprietary analysis package developed at IKI¹ (see details in Krivonos et al., 2010, 2012a; Churazov et al., 2014). Below we describe details of the data analysis that are relevant for the current work.

We first applied the energy calibration for the registered *IBIS/ISGRI* detector events with the “Off-line Scientific Analysis” (OSA) software package provided by the *INTEGRAL* Science Data Centre (ISDC) for Astrophysics² up to the COR level. We used the latest OSA version 11.2, which provides energy calibration for the whole period of observations.

We screened the data before subsequent analysis to reduce systematic noise and remove all contaminated observations and observations with insufficient statistics. If an individual *INTEGRAL* observation (*ScW* – “science window”) did not satisfy all the imposed criteria it was skipped. We screened all *ScWs* near the beginning and end of *INTEGRAL* revolution with orbital phases <0.2 or >0.8 , due to increased background near the radiation belts; the data when *IBIS* was operated not in its main regime (modes 41 and 43); and *ScWs* with exposure times less than 700 s. As a result, 131440 *ScWs* satisfies the selection criteria, with the total (dead-time corrected) exposure of 226 Ms.

Due to the loss of *ISGRI* sensitivity at low energies caused by the ongoing detector degradation, we define our energy bands above 25 keV. To characterize Galactic X-ray background we use three wide energy bands. First, the lower band

25–60 keV is chosen to better fit the spectrum of the GRXE, which has a cutoff at energies $\sim 30 - 50$ keV due to the typical cutoff in spectra of magnetic CVs (Suleimanov et al., 2005). Second, the intermediate 60–80 keV band is selected as interval, where the transition between GRXE and γ -ray background is observed. Third, the 80–200 keV band is selected as dominated by contribution of the γ -ray background.

For the spectral analysis, we selected 21 logarithmically spaced energy bands between 25 and 185 keV. We use the diagonal energy redistribution matrix which reproduces the Crab-like spectrum, represented as $10.0 \times E^{-2.1}$ keV photons $\text{cm}^{-2} \text{s}^{-1} \text{keV}^{-1}$ (see, e.g. Churazov et al., 2007).

3. *IBIS* telescope coding aperture

The coded-aperture paradigm implemented for the *IBIS* telescope does not allow directly investigate extended structures, which are significantly greater than the pixel size. However, Krivonos et al. (2007) showed that the *IBIS* telescope can be used for GRXE studies as a collimated instrument, which collects an emission from the both point sources and Galactic background, and the last can be measured separately after taking the internal detector background into account.

To work in a collimated mode, we do not need to visualize sky of each *ScW*, i.e. to apply standard coded-aperture image reconstruction. However, we subtract shadowgrams illuminated by a point sources from the detector plane using the known mask pattern (see details in Krivonos et al., 2010). The list of X-ray sources is taken from the recent 17-year *INTEGRAL/IBIS* all-sky survey (Krivonos et al., 2022). Hereafter we consider only ‘clean’ *ISGRI* detector count rate after removal of the contribution of point-like X-ray sources.

We additionally screened the data in each energy band for strong outliers (X-ray bursts, insufficient subtraction of bright sources and X-ray transients, interactions with heavy cosmic ray particles, etc.) in the observed detector count rate using an iterative 4σ clipping algorithm. After this step, the *ISGRI* detector count rate in each *ScW*, contains three components:

1. Cosmic X-ray Background (CXB, see e.g. Revnivtsev et al., 2003; Churazov et al., 2007; Krivonos et al., 2021);
2. Galactic X-ray Background (GXB), if the field of view of the telescope is directed towards the Galactic plane; Since we work in the energy range from 25 to 200 keV, hereafter, we refer to GXB as containing hard X-ray background (i.e. GRXE) below 60 keV and Galactic soft γ -ray background, starting to dominate above 80 keV.
3. detector internal background, caused by different processes including activation of different elements of the spacecraft, interaction of the detector material with cosmic-rays, etc. (Terrier et al., 2003).

The measurement of the surface brightness of the GXB subtended by the *IBIS* FOV is defined as the difference between the observed detector count rate for each *ScW* and the count rate predicted by the background model (Appendix A), and divided by the smooth polynomial function of the observed Crab count

¹Space Research Institute (IKI), Moscow, Russia

²<https://www.isdc.unige.ch/integral>

rate (Appendix B). The resulting value is, therefore, expressed in Crab (or mCrab) units, which can be converted to physical units ($\text{erg s}^{-1} \text{cm}^{-2}$) using Crab spectral model (Appendix B).

4. Results

4.1. Flux measurement

We defined three Galactic regions to measure X-ray flux, as listed in Table 1. The first region effectively includes X-ray emission of the Galactic Bulge (GB), the inner few kpc of our Galaxy (Dwek et al., 1995; Zoccali and Valenti, 2016). Two nearby “L+20” and “L−20” regions approximately cover Scutum and Norma Galactic spiral arms, respectively. Both L+20 and L−20 approximately cover the structure of the Galactic disk at $|l| < 50^\circ$, containing the main stellar mass component of the Galaxy. We additionally defined high-latitude 3C 273 and the Coma cluster region to test flux measurement procedure. This region has been the target of the deepest exposure with *INTEGRAL* extragalactic surveys (Krivonos et al., 2005; Paltani et al., 2008; Mereminskiy et al., 2016).

As described in Appendix A, to measure the X-ray surface brightness per *IBIS* FOV in a given sky region, we run Gaussian fitting procedure to estimate best-fitting mean flux value and its error. Table 1 contains the flux values, obtained by this approach for different sky regions.

The Galactic X-ray background is significantly detected in the GB region in all energy bands up to 200 keV. In 25–60 keV band, the GRXE flux in spiral arms is a factor of 2 lower than in the GB, which is consistent with NIR intensity distribution convolved with *IBIS/ISGRI* collimator response function (see Fig. 11 in Krivonos et al., 2007). In the intermediate 60–80 keV and γ -ray band 80–200 keV, the measured flux in spiral arms is detected at 3 – 6 σ confidence.

4.2. Morphology

We constructed longitude profile of the Galactic background emission. As we used the *IBIS/ISGRI* telescope with FOV of $\sim 15^\circ \times 15^\circ$ (FWHM) as a collimated instrument, the angular resolution of our resulting profile is approximately $\sim 15^\circ$. We defined longitude bins with a width of 15° and latitude height of $|b| < 10^\circ$. *INTEGRAL* observations within each region have been used to estimate X-ray flux as described in Sect. 4.1. In Fig. 1 we show longitude profiles for three energy bands.

We constructed the map of the Galaxy in the near infrared (NIR) spectral band at $4.9 \mu\text{m}$ using data of COBE/DIRBE observations, as described in Krivonos et al. (2007). The map of the NIR intensity was convolved with the *IBIS/ISGRI* collimator response function. The Galactic longitude profile of the COBE/DIRBE NIR intensity are shown by the solid line in Fig. 1 for 25–60 keV band. Note that NIR intensity was arbitrary scaled to approximately match the X-ray data. As seen from the figure, the 25–60 keV intensity distribution closely follows the NIR intensity, and thus traces the stellar mass density in the Galaxy.

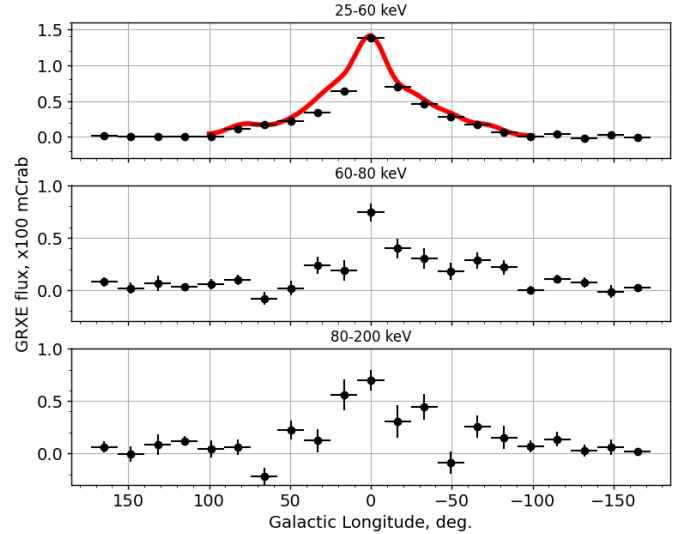


Figure 1: Galactic longitude profiles of Galactic X-ray Background in three energy bands. Red solid line represents intensity profile of the Galactic NIR emission obtained by COBE/DIRBE at $4.9 \mu\text{m}$. The NIR map was convolved with the *IBIS* collimator response.

4.3. Spectrum of the Galactic X-ray background

In Fig. 2 we show raw X-ray spectra of Galactic X-ray Background in mCrab units (see Sect. 4.1) in sky regions defined in Table 1. The brightest intensity is observed, as expected, in GB region. The X-ray intensity of spiral arms (L+20 and L−20) are similar to each other and a factor of ~ 2 less than that observed in the GB. To compare with, the measured X-ray intensity of the extragalactic field 3C 273/Coma is consistent with zero.

The spectral shape of the Galactic X-ray Background is a main source of information about its composition. We model 25–185 keV spectrum with two components. The stellar origin is expected at energies below 50–60 keV (GRXE), and γ -ray background is expected to dominate above 80 keV. We first modeled 25–185 keV spectrum by a combination of a power-law with photon index Γ^{cut} and high-energy cutoff E_{cut} (cutoffpl), representing GRXE, and a power-law with Γ^{pow} of γ -ray background. To be consistent with previous studies, we select $\Gamma^{\text{cut}} = 0$ and $\Gamma^{\text{pow}} = 1.55$, according to *INTEGRAL*/SPI study of the Galactic diffuse emission by Bouchet et al. (2008), also consistent with the results of later works (Türler et al., 2010; Bouchet et al., 2011; Siebert et al., 2022).

We run spectral fitting procedure with the following free parameters: the normalization of both power-law components, and high-energy cut-off E_{cut} . The normalization of each component has been estimated with *cflux* model in *xspec* in 30–80 keV energy band. The best fitting parameters are listed in Table 2. This spectral model gives good description of the data with a $\chi^2_{\text{red}} = 0.9 - 1.5$ for 18 d.o.f. In Fig. 3 we illustrate X-ray spectra and best-fit spectral models for three Galactic regions.

To describe the hard X-ray emission below $\sim 50 - 60$ keV with a physically motivated model, we use a one-dimensional accretion flow model that accounts for the density and temperature profile of the accretion column of intermediate polars (IPs)

Table 1: Description of sky regions, statistics of available observations and measured X-ray flux of Galactic X-ray background.

Name	Lon deg.	Lat deg.	Size ^{a)}	ScWs	Exp. Ms.	Flux ^{b)} (mCrab FOV ⁻¹)		
						25–60 keV	60–80 keV	80–200 keV
GB	0°	0°	6° × 6°	6697	9.8	154.9 ± 3.1	96.5 ± 9.2	102.2 ± 13.3
L+20	+20°	0°	20° × 10°	3160	4.3	69.1 ± 2.3	23.0 ± 5.2	56.7 ± 9.8
L–20	–20°	0°	20° × 10°	5068	7.7	67.9 ± 1.7	33.3 ± 5.3	29.3 ± 9.8
3C 273/Coma	–70°	70°	40° × 40°	5400	11.7	–1.0 ± 0.7	1.6 ± 2.0	5.6 ± 3.4

a) The centers of *INTEGRAL* observations are selected within the rectangular regions with specified size. Note that the *IBIS* FOV, used as a collimated instrument is $\sim 15^\circ \times 15^\circ$ (FWHM).

b) The flux is measured within *IBIS* FOV with effective solid angle $\Omega \approx 286 \text{ deg}^2$.

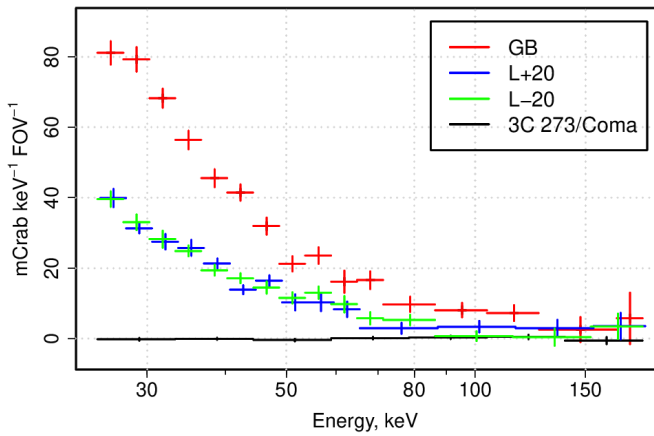


Figure 2: The X-ray spectra in mCrab units per *IBIS* FOV observed in different sky regions (Table 1). L+20 and L–20 spectra are shifted with respect to each other for better visibility.

Table 2: Best-fitting parameters of the model *cutoffpl+pow*.

Parameter	GB	L+20	L-20
Γ^{cut} (fixed)	0.0	0.0	0.0
E_{cut} , keV	11.2 ± 0.9	11.2 ± 1.5	11.2 ± 1.7
$F_{30-80 \text{ keV}}^{\text{cut}}$ ^{a)}	9.7 ± 1.4	4.3 ^{+1.2} _{-1.0}	4.3 ^{+1.1} _{-0.9}
Γ^{pow} (fixed)	1.55	1.55	1.55
$F_{30-80 \text{ keV}}^{\text{pow}}$ ^{a)}	4.9 ± 1.4	1.7 ± 1.3	2.2 ^{+1.0} _{-1.1}
$F_{30-80 \text{ keV}}^{\text{total}}$ ^{a)}	14.6 ± 0.2	6.1 ± 0.1	6.5 ± 0.1
$F_{30-80 \text{ keV}}^{\text{cut}}/F_{30-80 \text{ keV}}^{\text{total}}$	0.66 ± 0.10	0.70 ± 0.57	0.66 ± 0.37
$F_{30-80 \text{ keV}}^{\text{pow}}/F_{30-80 \text{ keV}}^{\text{total}}$	0.33 ± 0.10	0.27 ± 0.20	0.34 ± 0.14
$\chi_{\text{red}}^2/\text{dof}$	0.89/18	1.47/18	1.13/18

a) The flux is expressed in units $10^{-10} \text{ erg s}^{-1} \text{ cm}^{-2} \text{ FOV}^{-1}$

Table 3: Best-fitting parameters of the model *IPM+pow*.

Parameter	GB	L+20	L-20
M_{WD} , M_{\odot}	0.70 ± 0.09	0.73 ± 0.14	0.80 ± 0.15
$F_{30-80 \text{ keV}}^{\text{IPM}}$ ^{a)}	10.7 ^{+1.9} _{-1.7}	5.1 ± 1.4	5.6 ± 1.5
Γ^{pow} (fixed)	1.55	1.55	1.55
$F_{30-80 \text{ keV}}^{\text{pow}}$ ^{a)}	4.0 ± 1.7	1.1 ^{+1.4} _{-1.1}	1.1 ^{+1.4} _{-1.1}
$F_{30-80 \text{ keV}}^{\text{total}}$ ^{a)}	14.7 ± 0.2	6.2 ± 0.1	6.7 ± 0.1
$F_{30-80 \text{ keV}}^{\text{IPM}}/F_{30-80 \text{ keV}}^{\text{total}}$	0.73 ± 0.13	0.82 ± 0.23	0.83 ± 0.22
$F_{30-80 \text{ keV}}^{\text{pow}}/F_{30-80 \text{ keV}}^{\text{total}}$	0.27 ± 0.11	0.17 ± 0.22	0.16 ± 0.20
$\chi_{\text{r}}^2/\text{dof}$	0.76/18	1.27/18	0.83/18

a) The flux is expressed in units $10^{-10} \text{ erg s}^{-1} \text{ cm}^{-2} \text{ FOV}^{-1}$

developed by Suleimanov et al. (2005), which are the dominant contributors in hard X-rays. We use this IP model (IPM) to derive the average WD mass implied by our GB, L+20 and L–20 spectra. The IPM model has two parameters M_{WD} and normalization. By repeating the fitting procedure as described above, we estimated optimal model parameters listed in Table 3. The estimated average WD mass for all Galactic regions is consistent with each other within the uncertainties, and in good agreement with previous estimates $M_{\text{WD}} \approx 0.5 - 0.66 M_{\odot}$ (Krivonos et al., 2007; Türler et al., 2010; Yuasa et al., 2012; Heard and Warwick, 2013; Perez et al., 2019).

In contrary to our first work by Krivonos et al. (2007), when the measured spectrum of Galactic X-ray Background was characterized by a high-energy cutoff at $\sim 50 \text{ keV}$, we detect significant emission in the intermediate 60–80 keV band, and derived spectrum reveals a minimum at about 80 keV, as it was demonstrated by many works later on (Türler et al., 2010; Bouchet et al., 2008; Yuasa et al., 2012). We attribute the high-energy cut-off reported by Krivonos et al. (2007) to low statistics and unaccounted systematics, which resulted to somewhat underestimation of GRXE temperature, and consequently, the estimate of average mass of accreting WDs. The current analysis confirms the higher WD mass at the level of $\sim 0.7 M_{\odot}$.

5. Summary and conclusions

In this work we studied large-scale morphology and spectral properties of the Galactic hard X-ray and soft γ -ray Back-

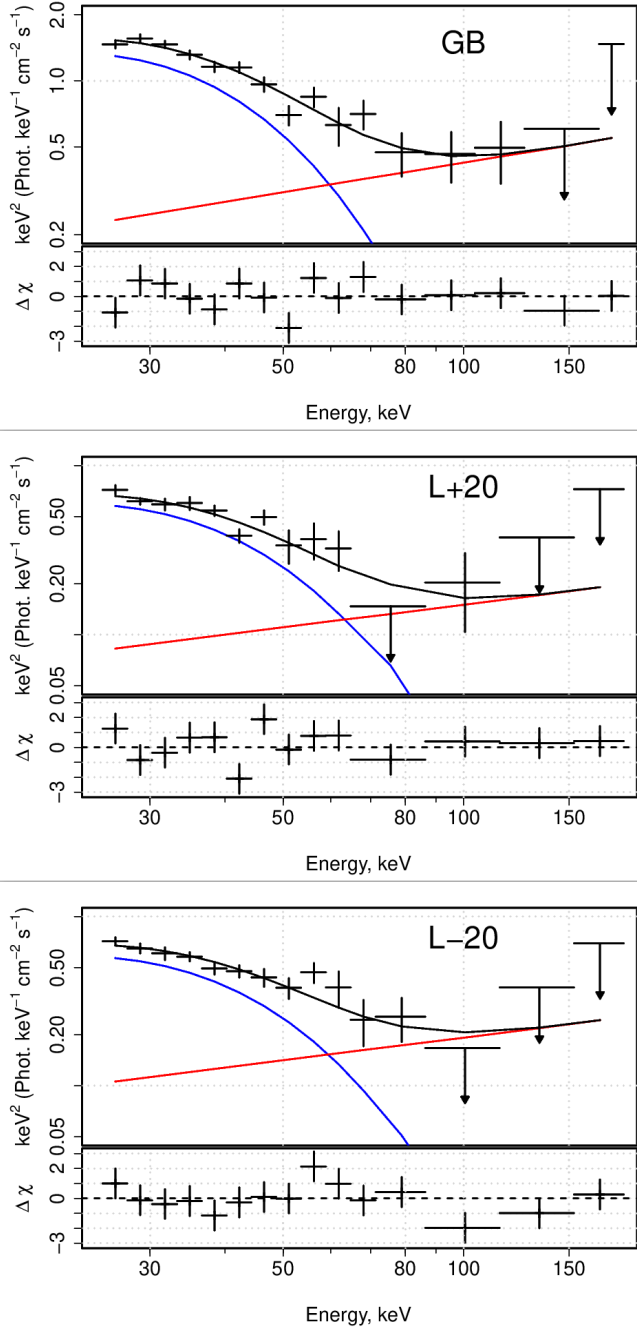


Figure 3: X-ray spectra of Galactic X-ray background in different Galactic regions (Table 1). The spectral modelling is done with a combination of power-law with a high-energy cut-off (*cutoffpl*, in blue) and a power-law with $\Gamma=1.55$ (red). For better plotting, no more than three adjacent spectral bins are combined to have 3σ detection. The upper limits are shown at the level of 2σ . The spectral flux is measured within the *IBIS* FOV with effective solid angle of $\Omega \approx 286 \text{ deg}^2$.

ground emission from 25 to 200 keV using multi-year *INTEGRAL* data. The aim of this work is to provide a model-independent measurement of large-scale extended emission of the Milky Way in the problematic domain of observations. We developed continuously-calibrated *IBIS/ISGRI* detector background model, characterized by $\sim 1-2\%$ systematic uncertainty, which allowed us to measure the distribution of X-ray intensity within the Galactic plane ($|l| < 90^\circ$, $|b| < 30^\circ$).

In the hard X-ray band 25–60 keV, the Galactic background is significantly detected in the region of Galactic bulge at the level of $\sim 155 \text{ mCrab}$ per *IBIS* FOV, represented by effective solid angle of 286 deg^2 . The measured flux in the Galactic disk is a factor of two less of this value, which is consistent with NIR intensity distribution. More detailed comparison of 25–60 keV longitude profile with NIR intensity, shows excellent agreement, indicating stellar origin of GRXE, as demonstrated by previous studies.

In the intermediate 60–80 keV band, the Galactic background emission is significantly (10σ) detected in the bulge region with flux $\sim 100 \text{ mCrab FOV}^{-1}$. The emission of the Galactic disk is measured at the level of $\sim 30 \text{ mCrab FOV}^{-1}$ with $4-6\sigma$ confidence. The longitude morphology within $|l| < 50^\circ$ is not peaked as NIR intensity and appears flattened, indicating different origin, most likely the growing contribution of the cosmic-ray induced γ -ray background.

In the soft γ -ray band 80–200 keV, the Galactic emission is detected in the bulge at the level of $\sim 100 \text{ mCrab FOV}^{-1}$ (8σ). The emission of the Galactic disk at $|l| < 50^\circ$ is detected with flux at the level of $\sim 30 - 60 \text{ mCrab FOV}^{-1}$ at low confidence ($3-6\sigma$).

The spectral analysis at energies between 25 and 185 keV reveals two distinct spectral components with a minimum at about 80 keV, as previously observed by different experiments. The low-energy component below $\sim 50-60 \text{ keV}$, coming from GRXE, is well described by a power-law model $\Gamma = 0$ with a high-energy cut-off $E_{\text{cut}} \approx 11 \text{ keV}$, and consistent with a one-dimensional accretion flow model of intermediate polars with an average WD mass of $M_{\text{WD}} \approx 0.7 M_\odot$. The high-energy part of the spectrum, attributed to γ -ray background at $E \gtrsim 80 \text{ keV}$ is consistent with a power-law model characterized by the photon index $\Gamma = 1.55$, as measured with early *INTEGRAL/SPI* studies. The total 30–80 keV flux budget observed with *IBIS/ISGRI* in the region of Galactic center $(14.7 \pm 0.2) \times 10^{-10} \text{ erg s}^{-1} \text{ cm}^{-2} \text{ FOV}^{-1}$, consists of $\sim 2/3$ of GRXE and $\sim 1/3$ of γ -ray background with *cutoffpl* model (Table 2). This ratio is observed at the same level for Galactic disk within the uncertainties. For IPM model, the fraction of GRXE in the total flux budget is higher ($\sim 80\%$, Table 3).

Finally, we provide the code of the *IBIS/ISGRI* background model used in this work as a Python module available in Git repository hosted by IKI³. The package contains *ISGRI* detector count rate cleaned from the contribution of X-ray point sources, for each ScW in the range of the *INTEGRAL* orbits 70–2740 and in different energy bands, used in this work. This data set

³<http://heagit.cosmos.ru/integral/ridge>

and code can be used to calibrate the *ISGRI* background model and measure the X-ray intensity of the Galactic background in different parts of the Milky Way.

Acknowledgements

Dedicated to Mikhail Revnivtsev (1974-2016). This work is based on observations with *INTEGRAL*, an ESA project with instruments and the science data centre funded by ESA member states (especially the PI countries: Denmark, France, Germany, Italy, Switzerland, Spain), and Poland, and with the participation of Russia and the USA. The authors are grateful to E. M. Churazov, who developed the *INTEGRAL*/*IBIS* data analysis methods and provided the software. This work was financially supported by grant 24-22-00212 from the Russian Science Foundation.

Appendix A. *ISGRI* detector background model

The aim of this work is to estimate the flux of the Galactic hard X-ray and soft γ -ray astrophysical background, which is in fact the difference between the observed total *ISGRI* source-free detector count rate and the predicted internal background when *IBIS* telescope is pointed towards the Milky Way. Note that the contribution of CXB is considered as a constant addition to the internal detector background (see Krivonos et al., 2007, for details) and hence not recognized as separate component in this work.

To predict the internal detector background in a given energy band, we apply a simple approach of measuring detector count rate when *INTEGRAL* performs observations at high Galactic latitudes, where contribution from the GXB is negligible.

We divided the sky into the two areas: GAL ($|l| < 90^\circ$, $|b| < 30^\circ$), which contains GXB, and BKG ($|l| \geq 90^\circ$, $|b| \geq 30^\circ$), used to trace the detector background. GAL and BKG sky regions contain 70226 and 61214 observations, with a total exposure of 112 and 114 Ms, respectively.

The background model implements a simple approach based on tracking detector count rate during each *INTEGRAL* orbit (~ 3 days). We assume that in-orbit variation of the background can be approximated by a linear law as a function of orbital phase Φ_{orb} within the range 0.2–0.8. Depending on the number of available BKG observations N_{BKG} within each orbit, we consider the following three options:

- $N_{\text{BKG}} \geq 10$ and the phase difference between first and last BKG observation is greater than 0.4: the background model is based on the linear regression $\alpha \times \Phi_{\text{orb}} + \beta$, which also provides the uncertainty of the model.
- $3 < N_{\text{BKG}} < 10$: the background model is a constant value, estimated as a mean of detector count rate over the corresponding BKG observations. The error is calculated from a standard deviation.
- $N_{\text{BKG}} < 3$: The background model is calculated as a linear interpolation between two closest orbits with a background model calibrated by one of two above cases. The

uncertainty is also estimated by interpolation. Obviously, this option triggered when no BKG observations are available during a given orbit.

Some *INTEGRAL* orbits, satisfied to the first condition, demonstrate rapid evolution of detector count rate, usually attributed to the observation of very bright X-ray source in outburst. Based on the distribution of the slope α , we additionally filtered out 673 orbits by condition $-2 \times 10^{-3} < \alpha < 10^{-3}$ cts $\text{s}^{-1} \text{pix}^{-1}$, resulting in 68406 and 56996 of GAL and BKG observations with exposure of 109 and 107 Ms, respectively.

Since the background model is based on high latitude observations (BKG region), the smooth work of it depends on how BKG observations located among GAL observations. Ideally, BKG observations should be uniformly distributed among GAL data. For instance, the multi-year program of Galactic latitude scans (PI: Sunyaev) designed for GRXE study, contains Galactic and high-latitude observations during one orbit in order to trace background variations. Unfortunately for this study, the typical *INTEGRAL* observational program is mainly concentrated within the Galactic plane without high-latitude background measurements. In the paradigm of the current background model, a number of GAL observations were made without representative nearby detector background, and GXB measurement is done with significant over- or under-estimation of the detector background. This is mainly seen as a step-like behaviour in the residuals per orbit time interval. This effect increases the systematic noise and must be taken into account. To do this, we performed additional filtering of the data as described in the following. We constructed light-curve of the residuals (observed minus predicted count rate) with time bin of one orbit. Then, we accumulated the distribution of the residuals. The distribution is characterized by a narrow peak and wide wings. To suppress the wings, we applied 3σ iterative clipping algorithm. We performed this procedure over all data set (GAL+BKG) in the last energy interval of spectral binning (168–185 keV). At these energies the effective area of the *ISGRI* detector is small, and the detector count rate is expected to be dominated by the internal detector background. As a result, we excluded 231 orbits from the analysis. The final data set contains 58474 and 55619 of GAL and BKG observations with exposure of 94 and 105 Ms, respectively.

In Fig. A.4 we show *ISGRI* detector count rate in three energy bands extracted from BKG sky region as a function of *INTEGRAL* orbit, along with prediction of the background model. Note that the noticeable two-humped variation is determined by the solar cycle, as also traced by the *INTEGRAL* γ -ray spectrometer SPI, by its anti-coincidence shield system (Diehl et al., 2018) and count rate of the instrumental lines (Siegert et al., 2022).

The distribution of residuals between the detector count rate and predicted background is shown in relative residuals (Fig. A.5) and in absolute flux (Fig. A.6) by using Crab calibration (Appendix Appendix B). As shown from the figures, the distribution is characterized by a narrow peak and wide wings, not described by a Gaussian function. Nevertheless, the residuals scatter around zero with a standard deviation of 27, 102,

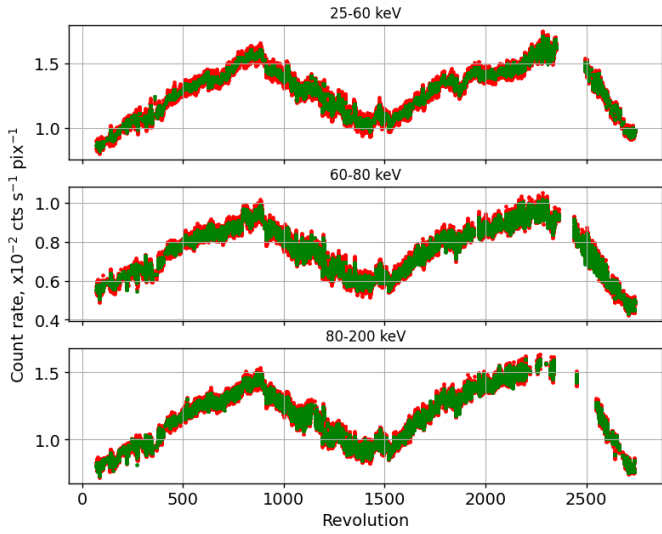


Figure A.4: *IBIS/ISGRI* detector count rate from BKG region (red points) and the count rate predicted by the background model (green points).

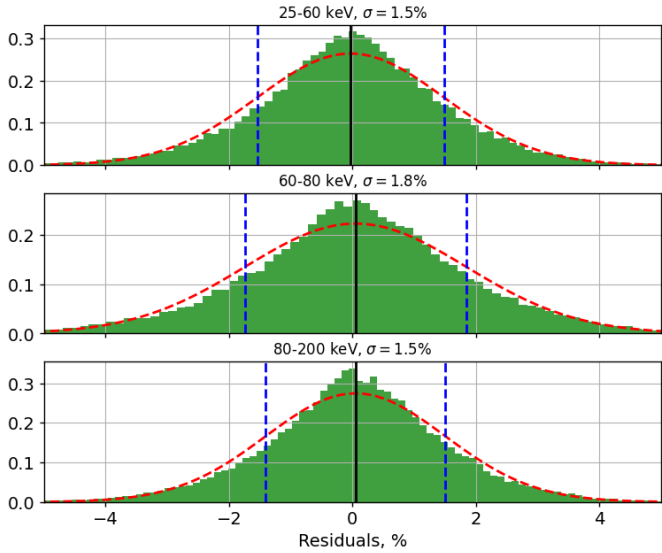


Figure A.5: Normalized distribution of the relative residuals of the background model obtained in three energy bands (BKG region, light-curve is shown in Fig. A.4). Dashed red line shows the best-fitting Gaussian function. Vertical solid line and dashed lines represent the best-fitted mean μ and standard deviation σ of the Gaussian function, respectively.

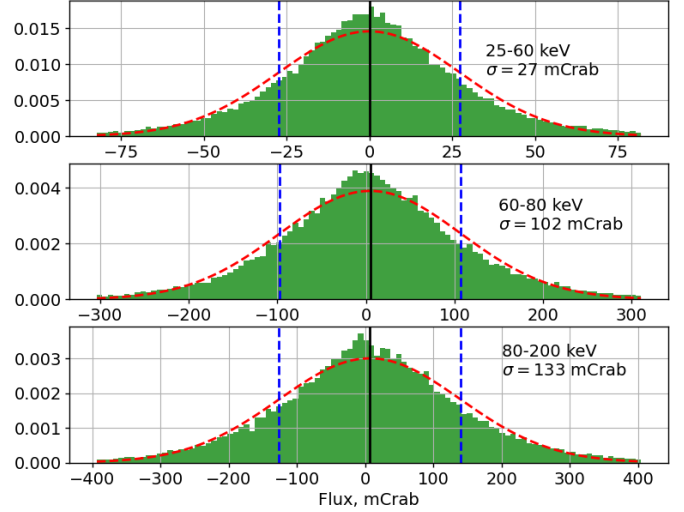


Figure A.6: Similar to Fig. A.5, normalized distribution of the residuals expressed in absolute flux units (mCrab).

and 133 mCrab in corresponding energy bands 25–60, 60–80 and 80–200 keV. Relative accuracy $<2\%$ indicates a sufficiently well-described background model.

In this work we measure the X-ray surface brightness in a given sky region by fitting the distribution of residuals described above with a Gaussian function. The position μ of the Gaussian provides the flux per *IBIS* FOV. The uncertainty of the flux is calculated as $\sigma \times N_{\text{scw}}^{-1/2}$, where σ is a best-fitted width of the Gaussian, and N_{scw} is a number of used *INTEGRAL* observations. To take the wide wings into account, we added a constant function with free normalization below and above μ . The break at μ is chosen to describe the wing's asymmetry observed in some cases.

Appendix B. *IBIS/ISGRI* Crab calibration

Krivonos et al. (2012b) estimated the effective solid angle of the *IBIS* telescope's FOV $\Omega \approx 286 \text{ deg}^2$ by integrating the *IBIS/ISGRI* collimator response function. The latter can be built by accumulating the shadowgram cast by Crab on the *ISGRI* detector as a function of angular offset. *IBIS/ISGRI* collimator response function, usually represented by a piece-wise linear function. The break position at $\sim 4.5 \text{ deg}$ corresponds to the division between $9^\circ \times 9^\circ$ fully coded and $29^\circ \times 29^\circ$ partially coded FOV of the *IBIS* telescope.

In this work, we measure the intensity of the GXB as an excess above the detector internal background within the effective solid angle Ω . The excess, expressed in terms of count rate ($\text{cts s}^{-1} \text{ pix}^{-1}$) in a given energy band, is converted to physical units ($\text{erg s}^{-1} \text{ cm}^{-2}$) using the observed count rate of Crab Nebula, a bright and stable X-ray source widely used in X-ray astronomy as a standard candle. The Crab spectrum can be approximated by a powerlaw, $dN/dE = N E^{-\Gamma}$ photon $\text{cm}^{-2} \text{ s}^{-1} \text{ keV}^{-1}$. In this work we use $N = 10$ and $\Gamma = 2.1$ to be compatible with our previous works, however recent Crab measurements are available (e.g., Madsen et al., 2017).

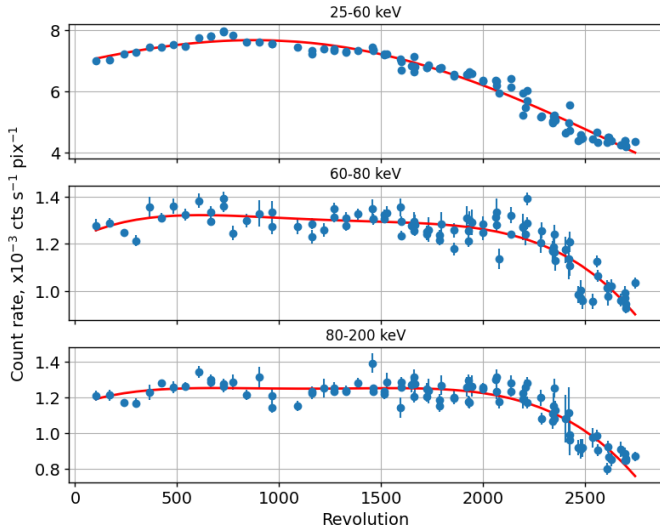


Figure B.7: The observed *IBIS/ISGRI* detector count rate of Crab Nebula (points). Red line represents cubic polynomial approximation.

Since we analyse multi-year *INTEGRAL* data, the observed count rate of Crab in a given energy band is subject to change due the long-term evolution of the detector efficiency. To trace this evolution, we selected *INTEGRAL* orbits for which at least ten Crab observations were carried out at angular distance less than 4.5 degrees. Fig. B.7 shows the average Crab count rate as a function of *INTEGRAL* revolution for 25–60, 60–80 and 80–200 keV bands. Assuming that the detector efficiency varies smoothly, we approximated the observed count rate with a cubic polynomial fit. The resulting function is used to convert the observed detector count rate in a given energy band for any *INTEGRAL* orbit into Crab units, and then, to physical flux.

To estimate the systematic uncertainty of this procedure, we accumulated the distribution of the residuals between the observed Crab count rate and polynomial fit for a given orbit in mCrab units, and approximated it with a Gaussian (see Fig. B.8). The standard deviation $\sigma = 37, 47$ and 44 mCrab, respectively, for 25–60, 60–80 and 80–200 keV band, is considered as a systematic uncertainty of the GRXE flux measurement. Note that it exceeds by at least an order of magnitude the statistical uncertainty estimated from the photon statistics. For this reason we decided to ignore statistical errors for GRXE measurements.

To summarize, the ratio between the *ISGRI* detector count rate at every every moment of time, in a given energy band and the corresponding polynomial value provides flux in Crab units measured within a solid angle subtended by the *IBIS* FOV.

References

- Bouchet, L., Jourdain, E., Roques, J.P., Strong, A., Diehl, R., Lebrun, F., Terrier, R., 2008. *INTEGRAL* SPI All-Sky View in Soft Gamma Rays: A Study of Point-Source and Galactic Diffuse Emission. *ApJ* 679, 1315–1326. doi:10.1086/529489, arXiv:0801.2086.
- Bouchet, L., Strong, A.W., Porter, T.A., Moskalenko, I.V., Jourdain, E., Roques, J.P., 2011. Diffuse Emission Measurement with the SPectrometer

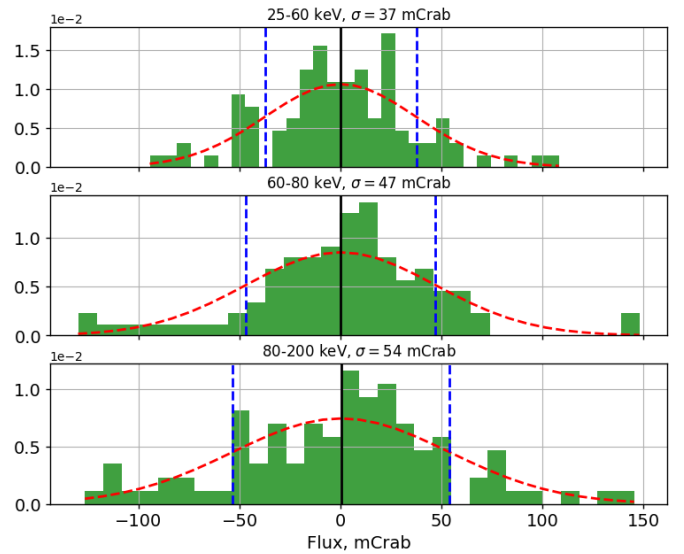


Figure B.8: The normalized distribution of the residuals between the *IBIS/ISGRI* Crab count rate (Fig. B.7) and the corresponding polynomial fit. The distribution is approximated with a Gaussian function. Vertical black solid and green dashed lines represent centroid of the distribution (consistent with zero) and standard deviation, respectively.

- on *INTEGRAL* as an Indirect Probe of Cosmic-Ray Electrons and Positrons. *ApJ* 739, 29. doi:10.1088/0004-637X/739/1/29, arXiv:1107.0200.
- Churazov, E., Sunyaev, R., Isern, J., Knödseder, J., Jean, P., Lebrun, F., Chugai, N., Grebenev, S., Bravo, E., Sazonov, S., Renaud, M., 2014. Cobalt-56 γ -ray emission lines from the type Ia supernova 2014J. *Nature* 512, 406–408. doi:10.1038/nature13672, arXiv:1405.3332.
- Churazov, E., Sunyaev, R., Revnivtsev, M., Sazonov, S., Molkov, S., Grebenev, S., Winkler, C., Parmar, A., Bazzano, A., Falanga, M., Gros, A., Lebrun, F., Natalucci, L., Ubertini, P., Roques, J.P., Bouchet, L., Jourdain, E., Knödseder, J., Diehl, R., Budtz-Jørgensen, C., Brandt, S., Lund, N., Westergaard, N.J., Neronov, A., Türler, M., Chernyakova, M., Walter, R., Produit, N., Mowlavi, N., Mas-Hesse, J.M., Domingo, A., Gehrels, N., Kukulers, E., Kretschmar, P., Schmidt, M., 2007. *INTEGRAL* observations of the cosmic X-ray background in the 5–100 keV range via occultation by the Earth. *A&A* 467, 529–540. doi:10.1051/0004-6361:20066230, arXiv:astro-ph/0608250.
- Diehl, R., Siebert, T., Greiner, J., Krause, M., Kretschmer, K., Lang, M., Pleintinger, M., Strong, A.W., Weinberger, C., Zhang, X., 2018. *INTEGRAL/SPI* γ -ray line spectroscopy. Response and background characteristics. *A&A* 611, A12. doi:10.1051/0004-6361/201731815, arXiv:1710.10139.
- Dwek, E., Arendt, R.G., Hauser, M.G., Kelsall, T., Lisse, C.M., Moseley, S.H., Silverberg, R.F., Sodroski, T.J., Weiland, J.L., 1995. Morphology, Near-Infrared Luminosity, and Mass of the Galactic Bulge from COBE DIRBE Observations. *ApJ* 445, 716. doi:10.1086/175734.
- Heard, V., Warwick, R.S., 2013. XMM-Newton observations of the Galactic Centre Region - I. The distribution of low-luminosity X-ray sources. *MNRAS* 428, 3462–3477. doi:10.1093/mnras/sts284, arXiv:1210.6808.
- Hunter, S.D., Bertsch, D.L., Catelli, J.R., Dame, T.M., Digel, S.W., Dingus, B.L., Esposito, J.A., Fichtel, C.E., Hartman, R.C., Kanbach, G., Kniffen, D.A., Lin, Y.C., Mayer-Hasselwander, H.A., Michelson, P.F., von Montigny, C., Mukherjee, R., Nolan, P.L., Schneid, E., Sreekumar, P., Thaddeus, P., Thompson, D.J., 1997. EGRET Observations of the Diffuse Gamma-Ray Emission from the Galactic Plane. *ApJ* 481, 205–240. doi:10.1086/304012.
- Karwin, C.M., Siebert, T., Beechert, J., Tomsick, J.A., Porter, T.A., Negro, M., Kierans, C., Ajello, M., Martinez-Castellanos, I., Shih, A., Zoglauer, A., Boggs, S.E., COSI Collaboration, 2023. Probing the Galactic Diffuse Continuum Emission with COSI. *ApJ* 959, 90. doi:10.3847/1538-4357/ad04df, arXiv:2310.12206.
- Kinzer, R.L., Milne, P.A., Kurfess, J.D., Strickman, M.S., Johnson, W.N., Pur-

- cell, W.R., 2001. Positron Annihilation Radiation from the Inner Galaxy. *ApJ* 559, 282–295. doi:10.1086/322371.
- Kniffen, D.A., Bertsch, D.L., Morris, D.J., Palmeira, R.A.R., Rao, K.R., 1978. Observations of medium-energy gamma-ray emission from the galactic center region. *ApJ* 225, 591–598. doi:10.1086/156519.
- Kraushaar, W.L., Clark, G.W., Garmire, G.P., Borken, R., Higbie, P., Leong, V., Thorsos, T., 1972. High-Energy Cosmic Gamma-Ray Observations from the OSO-3 Satellite. *ApJ* 177, 341. doi:10.1086/151713.
- Krivonos, R., Revnivtsev, M., Churazov, E., Sazonov, S., Grebenev, S., Sunyaev, R., 2007. Hard X-ray emission from the Galactic ridge. *A&A* 463, 957–967. doi:10.1051/0004-6361:20065626, arXiv:astro-ph/0605420.
- Krivonos, R., Revnivtsev, M., Tsygankov, S., Sazonov, S., Vikhlinin, A., Pavlinsky, M., Churazov, E., Sunyaev, R., 2010. INTEGRAL/IBIS 7-year All-Sky Hard X-ray Survey. I. Image reconstruction. *A&A* 519, A107. doi:10.1051/0004-6361/200913814, arXiv:1006.2463.
- Krivonos, R., Tsygankov, S., Lutovinov, A., Revnivtsev, M., Churazov, E., Sunyaev, R., 2012a. INTEGRAL/IBIS nine-year Galactic hard X-ray survey. *A&A* 545, A27. doi:10.1051/0004-6361/201219617, arXiv:1205.3941.
- Krivonos, R., Tsygankov, S., Revnivtsev, M., Sazonov, S., Churazov, E., Sunyaev, R., 2012b. INTEGRAL constraints on the Galactic hard X-ray background from the Milky Way anticenter. *A&A* 537, A92. doi:10.1051/0004-6361/201118053, arXiv:1109.2471.
- Krivonos, R., Vikhlinin, A., Churazov, E., Lutovinov, A., Molkov, S., Sunyaev, R., 2005. Extragalactic Source Counts in the 20–50 keV Energy Band from the Deep Observation of the Coma Region by INTEGRAL IBIS. *ApJ* 625, 89–94. doi:10.1086/429657, arXiv:astro-ph/0409093.
- Krivonos, R., Wik, D., Grefenstette, B., Madsen, K., Perez, K., Rosslund, S., Sazonov, S., Zoglauer, A., 2021. NuSTAR measurement of the cosmic X-ray background in the 3–20 keV energy band. *MNRAS* 502, 3966–3975. doi:10.1093/mnras/stab209, arXiv:2011.11469.
- Krivonos, R.A., Sazonov, S.Y., Kuznetsova, E.A., Lutovinov, A.A., Mereminskiy, I.A., Tsygankov, S.S., 2022. INTEGRAL/IBIS 17-yr hard X-ray all-sky survey. *MNRAS* 510, 4796–4807. doi:10.1093/mnras/stab3751, arXiv:2111.02996.
- Lebrun, F., Leray, J.P., Lavocat, P., Crétolle, J., Arquès, M., Blondel, C., Bonnin, C., Bouère, A., Cara, C., Chaleil, T., Daly, F., Desages, F., Dzitzko, H., Horeau, B., Laurent, P., Limousin, O., Mathy, F., Mau-guen, V., Meignier, F., Molinié, F., Poindron, E., Rouger, M., Sauvageon, A., Tourrette, T., 2003. Isgri: The integral soft gamma-ray imager *. *A&A* 411, L141–L148. URL: <https://doi.org/10.1051/0004-6361:20031367>, doi:10.1051/0004-6361:20031367.
- Lutovinov, A., Suleimanov, V., Manuel Luna, G.J., Sazonov, S., de Martino, D., Ducci, L., Doroshenko, V., Falanga, M., 2020. INTEGRAL View on cataclysmic variables and symbiotic binaries. *New A Rev.* 91, 101547. doi:10.1016/j.newar.2020.101547, arXiv:2008.10665.
- Madsen, K.K., Forster, K., Grefenstette, B.W., Harrison, F.A., Stern, D., 2017. Measurement of the Absolute Crab Flux with NuSTAR. *ApJ* 841, 56. doi:10.3847/1538-4357/aa6970, arXiv:1703.10685.
- Mereminskiy, I.A., Krivonos, R.A., Lutovinov, A.A., Sazonov, S.Y., Revnivtsev, M.G., Sunyaev, R.A., 2016. INTEGRAL/IBIS deep extragalactic survey: M81, LMC and 3C 273/Coma fields. *MNRAS* 459, 140–150. doi:10.1093/mnras/stw613, arXiv:1602.00463.
- Paltani, S., Walter, R., McHardy, I.M., Dwelly, T., Steiner, C., Courvoisier, T.J.L., 2008. A deep INTEGRAL hard X-ray survey of the 3C 273/Coma region. *A&A* 485, 707–718. doi:10.1051/0004-6361:200809450, arXiv:0805.0537.
- Perez, K., Krivonos, R., Wik, D.R., 2019. The Galactic Bulge Diffuse Emission in Broadband X-Rays with NuSTAR. *ApJ* 884, 153. doi:10.3847/1538-4357/ab4590, arXiv:1909.05916.
- Porter, T.A., Moskalenko, I.V., Strong, A.W., Orlando, E., Bouchet, L., 2008. Inverse Compton Origin of the Hard X-Ray and Soft Gamma-Ray Emission from the Galactic Ridge. *ApJ* 682, 400–407. doi:10.1086/589615, arXiv:0804.1774.
- Porter, T.A., Strong, A.W., 2005. A new estimate of the Galactic interstellar radiation field between 0.1um and 1000um, in: Acharya, B.S., Gupta, S., Jagadeesan, P., Jain, A., Karthikeyan, S., Morris, S., Tonwar, S. (Eds.), 29th International Cosmic Ray Conference (ICRC29), Volume 4, p. 77. doi:10.48550/arXiv.astro-ph/0507119, arXiv:astro-ph/0507119.
- Revnivtsev, M., Gilfanov, M., Sunyaev, R., Jahoda, K., Markwardt, C., 2003. The spectrum of the cosmic X-ray background observed by RTXE/PCA. *A&A* 411, 329–334. doi:10.1051/0004-6361:20031386, arXiv:astro-ph/0306569.
- Revnivtsev, M., Sazonov, S., Churazov, E., Forman, W., Vikhlinin, A., Sunyaev, R., 2009. Discrete sources as the origin of the Galactic X-ray ridge emission. *Nature* 458, 1142–1144. doi:10.1038/nature07946, arXiv:0904.4649.
- Revnivtsev, M., Sazonov, S., Forman, W., Churazov, E., Sunyaev, R., 2011. Luminosity function of faint galactic sources in the chandra bulge field: Faint galactic sources in cbf. *Monthly Notices of the Royal Astronomical Society* 414, 495–499. URL: <http://dx.doi.org/10.1111/j.1365-2966.2011.18411.x>, doi:10.1111/j.1365-2966.2011.18411.x.
- Revnivtsev, M., Sazonov, S., Gilfanov, M., Churazov, E., Sunyaev, R., 2006. Origin of the Galactic ridge X-ray emission. *A&A* 452, 169–178. doi:10.1051/0004-6361:20054268.
- Revnivtsev, M., Sazonov, S., Krivonos, R., Ritter, H., Sunyaev, R., 2008. Properties of the galactic population of cataclysmic variables in hard x-rays. *Astronomy and Astrophysics* 489, 1121–1127. URL: <http://dx.doi.org/10.1051/0004-6361:200810213>, doi:10.1051/0004-6361:200810213.
- Riegler, G.R., Ling, J.C., Mahoney, W.A., Wheaton, W.A., Jacobson, A.S., 1985. The Gamma-Ray Spectrum of the Galactic Center Region. *ApJ* 294, L13. doi:10.1086/184499.
- Siegert, T., Bertheaud, J., Calore, F., Serpico, P.D., Weinberger, C., 2022. Diffuse Galactic emission spectrum between 0.5 and 8.0 MeV. *A&A* 660, A130. doi:10.1051/0004-6361/202142639, arXiv:2202.04574.
- Strong, A.W., Diehl, R., Halloin, H., Schönfelder, V., Bouchet, L., Mandrou, P., Lebrun, F., Terrier, R., 2005. Gamma-ray continuum emission from the inner Galactic region as observed with INTEGRAL/SPI. *A&A* 444, 495–503. doi:10.1051/0004-6361:20053798, arXiv:astro-ph/0509290.
- Suleimanov, V., Revnivtsev, M., Ritter, H., 2005. RXTE broadband X-ray spectra of intermediate polars and white dwarf mass estimates. *A&A* 435, 191–199. doi:10.1051/0004-6361:20041283, arXiv:astro-ph/0405236.
- Terrier, R., Lebrun, F., Bazzano, A., Belanger, G., Bird, A.J., Blondel, C., David, P., Goldoni, P., Goldwurm, A., Gros, A., Laurent, P., Malaguti, G., Sauvageon, A., Segreto, A., Ubertini, P., 2003. In-flight calibration of the ISGRI camera. *A&A* 411, L167–L172. doi:10.1051/0004-6361:20031391, arXiv:astro-ph/0310096.
- Türler, M., Chernyakova, M., Courvoisier, T.J.L., Lubiński, P., Neronov, A., Produit, N., Walter, R., 2010. INTEGRAL hard X-ray spectra of the cosmic X-ray background and Galactic ridge emission. *A&A* 512, A49. doi:10.1051/0004-6361/200913072, arXiv:1001.2110.
- Ubertini, P., Lebrun, F., Di Cocco, G., Bazzano, A., Bird, A.J., Broenstad, K., Goldwurm, A., La Rosa, G., Labanti, C., Laurent, P., Mirabel, I.F., Quadrini, E.M., Ramsey, B., Reglero, V., Sabau, L., Sacco, B., Staubert, R., Vigroux, L., Weisskopf, M.C., Zdziarski, A.A., 2003. IBIS: The Imager on-board INTEGRAL. *A&A* 411, L131–L139. doi:10.1051/0004-6361:20031224.
- Winkler, C., Courvoisier, T.J.L., Di Cocco, G., Gehrels, N., Giménez, A., Grebenev, S., Hermsen, W., Mas-Hesse, J.M., Lebrun, F., Lund, N., Palumbo, G.G.C., Paul, J., Roques, J.P., Schnopper, H., Schönfelder, V., Sunyaev, R., Teegarden, B., Ubertini, P., Vedrenne, G., Dean, A.J., 2003. The INTEGRAL mission. *A&A* 411, L1–L6. doi:10.1051/0004-6361:20031288.
- Yuasa, T., Makishima, K., Nakazawa, K., 2012. Broadband Spectral Analysis of the Galactic Ridge X-Ray Emission. *ApJ* 753, 129. doi:10.1088/0004-637X/753/2/129, arXiv:1205.1574.
- Zoccali, M., Valenti, E., 2016. The 3d structure of the galactic bulge. *Publications of the Astronomical Society of Australia* 33. URL: <http://dx.doi.org/10.1017/pasa.2015.56>, doi:10.1017/pasa.2015.56.